frontiers in Energy Research

ORIGINAL RESEARCH
published: 07 June 2021
doi: 10.3389/fenrg.2021.689416

Co-Sintering Study of $Na_{0.67}[Ni_{0.1}Fe_{0.1}Mn_{0.8}]O_2$ and NaSICON Electrolyte–Paving the way to High Energy Density All-Solid-State Batteries

Gerald Dück[1,2†], Sahir Naqash[1,2,3†], Martin Finsterbusch[1,2,3], Uwe Breuer[4], Olivier Guillon[1,2,3] and Dina Fattakhova-Rohlfing[1,2,3,5]*

[1]Institute of Energy and Climate Research, Materials Synthesis and Processing (IEK-1), Forschungszentrum Jülich GmbH, Jülich, Germany, [2]Jülich Aachen Research Alliance, JARA-Energy, Jülich, Germany, [3]Helmholtz-Institute Münster, Forschungszentrum Jülich GmbH, Jülich, Germany, [4]Central Institute for Engineering, Electronics and Analytics (ZEA-3), Forschungszentrum Jülich GmbH, Jülich, Germany, [5]Faculty of Engineering and Center for Nanointegration Duisburg-Essen (CENIDE), Universität Duisburg-Essen, Duisburg, Germany

OPEN ACCESS

Edited by:
Candace K. Chan,
Arizona State University, United States

Reviewed by:
Manickam Minakshi,
Murdoch University, Australia
Vincent Seznec,
University of Picardie Jules Verne, France

***Correspondence:**
Gerald Dück
g.dueck@fz-juelich.de

†These authors have contributed equally to this work and share first authorship

Specialty section:
This article was submitted to Electrochemical Energy Conversion and Storage, a section of the journal Frontiers in Energy Research

Received: 31 March 2021
Accepted: 20 May 2021
Published: 07 June 2021

Citation:
Dück G, Naqash S, Finsterbusch M, Breuer U, Guillon O and Fattakhova-Rohlfing D (2021) Co-Sintering Study of $Na_{0.67}[Ni_{0.1}Fe_{0.1}Mn_{0.8}]O_2$ and NaSICON Electrolyte–Paving the way to High Energy Density All-Solid-State Batteries. Front. Energy Res. 9:689416. doi: 10.3389/fenrg.2021.689416

Sodium is a promising candidate for stationary storage applications, especially when the demand for lithium-ion batteries increases due to electromobility applications. Even though its energy density is lower, Na-ion technology is estimated to lead to a cost reduction of 30% compared to Li-ion technology. To improve safety as well as energy density, Na-based all-solid-state-batteries featuring solid electrolytes such as beta-alumina and sodium superionic conductors and cathode materials such as $Na_3V_2(PO4)_3$ and Na_xCoO_2 have been developed over the past years. However, the biggest challenge are mixed cathodes with highly conductive interfaces, especially when co-sintering the materials. For example, a promising sodium superionic conductor type $Na_3Zr_2Si_2PO_{12}$ electrolyte sinters at 1,250°C, whereas the corresponding $Na_3V_2PO_{12}$ cathode decomposes at temperatures higher than 900°C, posing a bottleneck. Thus in this paper, we synthesized $Na_{0.62}$ $[Ni_{0.10}Fe_{0.10}Mn_{0.80}]O_2$ as cathode material for all-solid-state sodium-ion batteries *via* a relatively cheap and easy solution-assisted solid state reaction processing route. The thermal investigations of the pure cathode material found no degradation up to 1,260°C, making it a perfect match for $Na_{3.4}Zr_2Si_{2.4}P_{0.6}O_{12}$ electrolyte. In our aim to produce a co-sintered mixed cathode, electron microscopy investigation showed a highly dense microstructure and the elemental mapping performed *via* energy dispersive X-ray spectroscopy and secondary ion mass spectrometry confirm that $Na_{3.4}Zr_2Si_{2.4}P_{0.6}O_{12}$ and $Na_{0.62}$ $[Ni_{0.10}Fe_{0.10}Mn_{0.80}]O_2$ do not react during sintering. However, the active cathode material forms a sodium rich and a sodium deficient phase which needs further investigation to understand the origin and its impact on the electrochemical performance.

Keywords: sodium, NASICON, solid electrolyte, solid-state-batteries, composite cathode

INTRODUCTION

In recent decades, lithium-ion batteries (LIB) have seen a significant increase in their technological advancement and economical importance (Zubi et al., 2018; Zeng et al., 2019; Avicenne, 2020). Their application in portable devices such as e.g., phones, household tools, and electric vehicles requires high performance as well as a high degree of safety. One approach to increase safety and energy density is by replacing the liquid with a more mechanically stable, heat and voltage resistant solid electrolyte (Mckissock et al., 2008; Finsterbusch et al., 2018). These so-called solid-state batteries (SSB) are at the initial stages of development which means more and more research is being carried out to develop cheaper and safer battery technology. Additionally, the environmental friendliness of LIB is also a concern due to the mining of raw materials and the carbon footprint involved in their production. While energy storage is not a general solution without de-carbonization of electricity generation, long cycle stability and the pursuit of finding environmentally friendly alternatives to lithium are significantly important (Larcher and Tarascon, 2015; Peters et al., 2016). Among alternatives, sodium is a promising candidate as it is 1,000 times more abundant than lithium in the Earth's crust, and this does not include seawater sodium. A high abundance leads to low material cost, e.g., Na_2CO_3 is approx. 60 times cheaper than Li_2CO_3 and the gap is widening with increasing demand for LIBs (Peters et al., 2019). In terms of performance, sodium is three times heavier than lithium (23 g mol^{-1} compared with 6.9 g mol^{-1}), and 0.3 V less electropositive, which means that gravimetric and volumetric penalties (~15%) are unavoidable. This makes sodium batteries ideal for applications where energy density is not the highest ranking performance indicator, e.g., in stationary storage applications (Yabuuchi et al., 2014). Especially, since early estimations for Na-ion technology forecast a cost reduction of 30% as compared to Li-ion technology (Larcher and Tarascon, 2015).

To combine both approaches, Na-SSBs featuring solid electrolytes such as beta-alumina and NaSICON (Ma and Tietz, 2020) and cathode materials such as $Na_3V_2(PO_4)_3$ (Gopalakrishnan and Rangan, 1992) and Na_xCoO_2 (Doeff et al., 1995) have been developed over the past years. The biggest challenge for SSB technology however is to fabricate a mechanically, electrochemically, and chemically stable electrode-electrolyte interface. Most of the available electrode and electrolyte materials have different sintering temperatures and different thermal expansion coefficients. This causes delamination of interfaces when cathode and electrolyte are co-sintered. For example, a promising NaSICON type $Na_3Zr_2Si_2PO_{12}$ electrolyte sinters at 1,250°C, whereas the corresponding NaSICON type $Na_3V_2PO_{12}$ cathode decomposes at temperatures higher than 900°C, posing a bottleneck (Lalère et al., 2014; Lan et al., 2019). Furthermore, research has gone into improving the contact between electrolyte and electrode, e.g., through laminating by applying a soft interlayer of polymers (Gao et al., 2018) or ionic liquids (Liu et al., 2016; Zhang et al., 2017). Although somewhat successful, the materials challenges associated with the interfaces in these systems still remains the major hurdle for achieving high-temperature stability and high voltage all-solid-state batteries with polymer or liquids. Ultimately, co-sintering remains the best option to fabricate a fully inorganic ASSB without the necessity for liquid or gel type additive in any form. The following characteristics are needed to obtain good inorganic cells (Inoishi et al., 2017);

1) Electrolyte and cathode should have similar sintering temperatures (if not the same),
2) Have similar thermal expansion coefficient to avoid cracking and
3) Be chemically stable.

An inherent problem of these systems, however, is the volume expansion and contraction of the active cathode material as Na ions are intercalated and de-intercalated during charging- and discharging-cycles (Zhang et al., 2017). The rigid electrode/electrolyte interface cannot sustain the constant volume change that leads to crack formation and increased polarization, which eventually degrades the cell capacity (Ma et al., 2019). One way to overcome this issue is by using a cathode material that has a negligible volume change during cycling. One such material has recently been reported by Choi et al. i.e., $Na_x[Ni_{0.1}Fe_{0.1}Mn_{0.8}]O_2$ and it has a volume change of only 3.3% during cycling (Choi et al., 2020).

Mn-based materials are low cost and simple to manufacture (Yabuuchi et al., 2014). Various MnO_2 based materials were investigated in detail for liquid based cells, e.g., by the Minakshi group (Minakshi and Ralph, 2013). The crystal structures and a Na-ion insertion/extraction-ability of sodiated manganese oxide ($Na_{1-x}MnO_2$) were earlier reported by Parent et al., (Parant et al., 1971). Among them, P'2-Na_xMnO_2 is stable even at temperatures as high as 1,000–1,200°C (Stoyanova et al., 2010), which is similar to that of NASICON solid electrolyte. This material has an initial discharge capacities of ~200 mA h g^{-1} in the voltage range of 1.5–4.4 V (Kumakura et al., 2016) when cycled at ~2.7 V (Choi et al., 2020). However, this material suffers strong volume changes during desodiation process and this structural instability leads to a gradual capacity fading (Choi et al., 2018; Choi et al., 2019). Choi et al. (Choi et al., 2020) recently reported that by doping Mn with Ni and Fe in P'2-Na_xMnO_2, volume change is reduced to only ~3.3% when cycled between fully sodiated and desodiated states. The composition of fully sodiated and desodiated state is P'2-$Na_{0.9}$ $[Ni_{0.1}Fe_{0.1}Mn_{0.8}]O_2$ and OP4-$Na_{0.07}$ $[Ni_{0.1}Fe_{0.1}Mn_{0.8}]O_2$ and their structure is shown in **Figure 1**. We opted for P'2-$Na_{0.67}$ $[Ni_{0.1}Fe_{0.1}Mn_{0.8}]O_2$ (NNFM) due to its high thermal and cycling stability and the high discharge capacity of 220 mA h g^{-1} reported in literature (Choi et al., 2020).

Among solid electrolytes, we chose a NASICON type composition $Na_{3.4}Zr_2Si_{2.4}P_{0.6}O_{12}$ (NZSiP) that has a conductivity of 5 $mScm^{-1}$ at room temperature (Ma et al., 2019). The sintering temperature of NZSiP is between 1,200 and 1,300°C, which matches the thermal stability window of NNFM. Therefore, we attempted to co-sinter the NNFM and NZSiP. In this study, we have investigated the thermal and

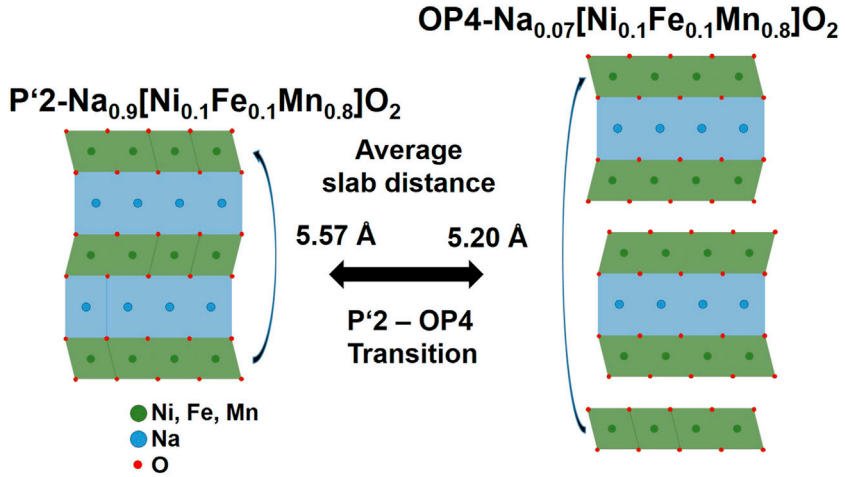

FIGURE 1 | Structural transition of NNFM from sodiated to de-sodiated state.

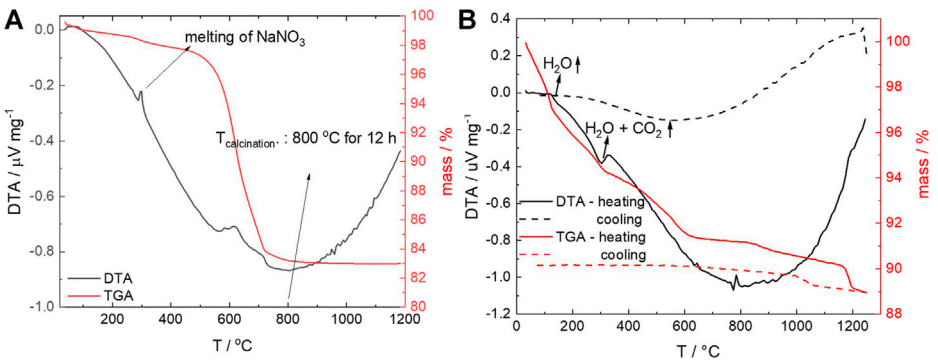

FIGURE 2 | DTA/TG analysis of NNFM pre-calcined at 500°C for 10 h in air **(A)** and of mixed NNFM/NZSiP **(B)**. Measurements performed in artificial air with a heating and cooling rate of 5 K/min.

chemical stability of NNFM as cathode and NZSiP as electrolyte material to fabricate a mixed cathode for potential use in all-solid-state battery.

MATERIALS AND METHODS

$Na_{3.4}Zr_2Si_{2.4}P_{0.6}O_{12}$ Synthesis

NZSiP was synthesized using the solution-assisted solid-state-reaction (SA-SSR) (Ma et al., 2016). Stoichiometric amounts of $NaNO_3$ (Merck, ACS), $ZrO(NO_3)_2 \bullet xH_2O$ (Sigma-Aldrich, techn. grade), Tetraethyl orthosilicate (Merck, ≥ 99%) and $NH_4H_2PO_4$ (Merck, ACS) were dissolved in deionized water at room temperature. The solution with formed precipitates was dried at 70°C and calcined at 800°C for 4 h with a heating and cooling rate of 5 K/min in air. The calcined powder was finally ball milled with a mixture of 3 and 5 mm zirconia balls (50:50 by weight) in ethanol for approx. 72 h or until a median particle size of 1–2 µm was reached.

$Na_{0.67}[Ni_{0.1}Fe_{0.1}Mn_{0.8}]O_2$ Synthesis

$Na_{0.67}$ $[Ni_{0.1}Fe_{0.1}Mn_{0.8}]O_2$ was synthesized via a SA-SSR route (Ma et al., 2016). Stoichiometric amounts of $Ni(NO_3)_2{\cdot}6$ H_2O (VWR, ACS), $Fe(NO_3)_2{\cdot}9$ H_2O (VWR, ACS), $Mn(NO_3)_2{\cdot}4$ H_2O (Merck, EMSURE), and $NaNO_3$ (Merck, ACS), with a 10% excess of Na to compensate for sodium loss, were dissolved in deionized water at room temperature. The solution was dried while stirring on a hotplate at 100°C. As described by Choi et al., (Choi et al., 2020), the formed powder was calcined at 500°C to remove the nitrates. Afterward, the powder was ground with mortar and pestle before calcining again at 800°C. Finally, the powder was uniaxially pressed into pellets with 13 mm diameter at 100 MPa for 2 min and further sintered at 1,200°C for 10 h or 1,260°C for 6 h in air.

The calcined powders of NZSiP and NNFM were mixed in a weight-ratio of 1 to 1 and ball milled together with a mixture of 3 and 5 mm ZrO_2 balls (50:50 by weight) in ethanol for 24 h. The resulting material was uniaxially pressed into pellets of 13 mm diameter with 100 MPa and sintered at 1,200°C for 10 h or

TABLE 1 | Analytical compositions after different heat treatments of NNFM. The obtained atomic ratios were normalized to one central cation per formula unit (Ni + Fe + Mn = 1).

Heat treatment (C)	Analytical composition (ICP-OES)
500	$Na_{0.742(10)}[Ni_{0.101(2)}Fe_{0.102(1)}Mn_{0.798(4)}]O_2$
800	$Na_{0.725(10)}[Ni_{0.103(1)}Fe_{0.101(1)}Mn_{0.796(4)}]O_2$
1,200	$Na_{0.618(10)}[Ni_{0.101(1)}Fe_{0.102(1)}Mn_{0.796(4)}]O_2$

1,260°C for 6 h in air to achieve dense pellets, in an attempt to produce a co-sintered all solid-state cathode material.

Characterization

Powder particle size distribution was measured by static laser light scattering technique (LA-950 V2, Retsch). The chemical compositions of the powders were analyzed by ICP-OES (Thermo Scientific iCAP7600 spectrometer with optical scale and CID semi-conductor detector, axial and radial reflection, wavelength 166–847 nm). Two 50 mg samples were each mixed with 0.25 g lithium borate and brought to melt in a Pt-crucible at 1,000°C for 30 min. The melts were dissolved in 30 ml HCl (5%) and with addition of 2 ml HF were filled to 50 ml. Of each sample two measurements were conducted with 1/100 and 1/10 dilution. The behavior of the powder on heating in artificial air (mixture N_2/O_2 of 80/20) was investigated by DTA/TG-MS (Netzsch, STA449 F1 Jupiter, and QMS 403C Aëolos). The crystal structure of $Na_{0.67}$ $[Ni_{0.1}Fe_{0.1}Mn_{0.8}]O_2$ was confirmed by X-ray diffraction (XRD, Bruker D4 ENDEAVOR diffractometer with Cu Kα-radiation).

Shrinkage behavior during sintering was investigated with dilatometry (402C Netzsch, Germany) on specimens prepared from powder precursors by uniaxial pressing at 100 MPa into round pellets of 8 mm diameter. Thermal expansion coefficient was investigated by push-rod dilatometer 402C from Netzsch, Germany, calibrated with a sapphire single crystal. NNFM and NZSiP specimens were prepared from powder precursors by uniaxial pressing with 150 MPa into a rectangular shape (40 mm × 5 mm × 3–5 mm) and subsequent sintering at 1,260°C. The terminal faces were then cut and polished to a sample length of 25 mm and then measured.

The co-sintered composite was further investigated with SEM and EDX (Carl Zeiss NTS GmbH, Zeiss Ultra 55 and Zeiss Supra 50 VP^2). TOF-SIMS analysis were performed by using TOF-SIMS V system (ION-TOF GmbH, Münster, Germany). The measurements were done in a dual beam setting (Iltgen et al., 1997) in non-interlaced mode (Dellen et al., 2016). For the materials erosion, a 1 keV oxygen ion beam was rasterized over an area of 300 μm^2 × 300 μm^2. For generation of analyzed secondary ions, a focused 25 keV Bi3 ion beam was used and the Bi ion gun was operated in the high current bunched mode. The analyzed area was 50 μm^2 × 50 μm^2 and centered within the sputter crater to avoid crater edge effects. Between the sputtering and analysis pulses, a low energy (20 eV) electron flood gun was used to compensate for sample charging during the sputter processes. The data analysis was carried out by using Software package SurfaceLab 6 (ION-TOF GmbH).

RESULTS AND DISCUSSION

Chemical Composition

The compositions determined by ICP-OES of NNFM after heat treatment at 500, 800, and 1,200°C are shown in **Table 1**. It confirms a minimal loss of ~1 mol% Na after calcining at 800°C, considering an experimental error of ± 3%. A higher 10 mol% Na loss is observed after sintering at 1,200°C and is due to the evaporation of sodium oxide and in agreement with (Choi et al., 2020). This is the reason why an excess of Na was used to synthesis the NNFM to achieve a final composition with stoichiometry close to $Na_{0.67}$ $[Ni_{0.10}Fe_{0.10}Mn_{0.80}]O_2$. Furthermore, for NZSiP, the elemental analysis confirmed a composition of $Na_{3.43(14)}Zr_{2.00}Si_{2.51(18)}P_{0.59(3)}O_{12}$ even after 1,260°C for 6 h.

Thermal Stability

To study the thermal stability of NNFM/NZSiP co-sintered samples, we first performed DTA/TG-MS analysis of a NNFM powder pre-calcined at 500°C as shown in **Figure 2A**. A gradual weight loss of around 3% up to 550°C is observed due to the removal of absorbed moisture and CO_2. A sharp weight loss is subsequently observed around 600°C which corresponds to a decomposition of sodium nitrate (Gordon and Campbell, 1955; Yuvaraj et al., 2003). From 800°C onwards, no further weight loss is observed which verifies the thermal stability of NNFM up to 1,200°C. For this reason, NNFM was calcined at 800°C to prepare a precursor material which can be subsequently used for co-sintering with the NZSiP. The calcined NNFM was then mixed with calcined NZSiP in a 50/50 ratio (w/w) and DTA/TG-MS analysis of the mixture was done. **Figure 2B** shows again a

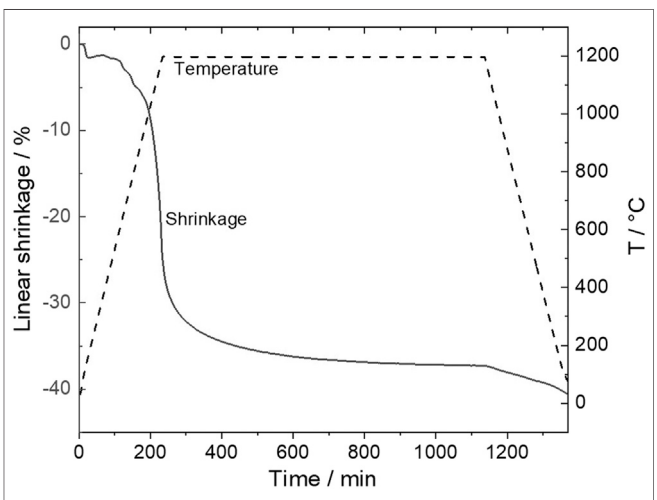

FIGURE 3 | Dilatometry of NNFM/NZSiP mixed material performed in artificial air with a heating rate of 5 K/min from 35 to 1,200°C, holding time of 10 h, followed by a cooling down to RT with 5 K/min.

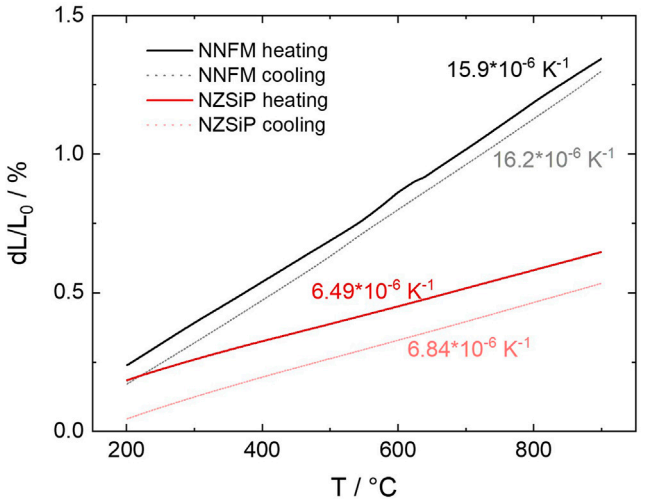

FIGURE 4 | Dilatometry of NNFM (black) and NZSiP (red) from 25 to 1,200°C with heating and cooling rate of 3 K/min and 30 min holding time at 1,200°C in air. CTE determined between 200 and 900°C.

gradual weight loss up to around 600°C due to removal of moisture and CO_2. Around 800°C we can observe another minor weight loss which could be due to oxidation of still leftover nitrates and a mass loss of just over 1% can be observed around 1,200°C. The high temperature mass loss is reversible, as we can see from the cooling curve. Therefore, this is most likely from oxygen removal in the oxide phase, which reinserts during cooling. However, measurements were performed in air, so oxygen removal from the sample could not be measured. Overall, DTA/TG-MS indicates no decomposition or reaction of the two materials.

The shrinkage behavior of an NZSiP and NNFM composite is shown in **Figure 3**. An overall shrinkage of more than 35% confirms a very good co-sinterability of these two materials.

Coefficient of Thermal Expansion

To further investigate the co-sinterability, the thermal expansion curve of the NNFM/NZSiP composite were measured on pre-sintered samples as shown in **Figure 4**. The hysteresis in the cooling and heating curves of the two samples indicate the influence of micro-cracks, which has already been described elsewhere (Naqash et al., 2018). The linear coefficients of thermal expansion CTE of NNFM and NZSiP were calculated using **Eq. 1**. The thermal expansion curve was linear only in the temperature range (ΔT) of 200–900°C therefore only the change of length (ΔL) during this temperature range was used. Here L_0 is the original length.

$$CTE = \frac{\Delta L}{\Delta T \cdot L_0} \quad (1)$$

NNFM has a CTE of around $16{\cdot}10^{-6}$ K^{-1} which is about 2.5 times the CTE of NZSiP. We observed minimal cracking between the NNFM and NZSiP grains in the microstructure of the NNFM/NZSiP composite (see microstructure section **Figure 5**). This is surprising since the CTE values are independent of crystal orientation. If the crystal anisotropy is considered, an even stronger CTE mismatch and therefore very high residual stresses in the composite could be expected (Mücke et al., 2021). Still, this difference in the CTE appears to be within an acceptable range that the mismatch can be tolerated.

Crystal Structure

The crystallographic investigations via XRD reveal that NNFM is only partially adapting a P'2-type $Na_{0.67}$ $[Ni_{0.1}Fe_{0.1}Mn_{0.8}]O_2$ crystal structure after calcination at 800°C (**Figure 6B**). A minor side phase can be observed showing a peak at 16.6° 2θ, which is unidentified due to its very low intensity. After sintering at 1,200°C, NNFM is fully crystallized and adapts a pure P'2 phase, as expected from (Choi et al., 2020). Furthermore, our investigation also reveals that pure NNFM is stable even up to 1,260°C and forms the desired phase (**Figure 6C**), which, to our knowledge, has not been reported so far.

After confirming the thermal stability of NNFM, the phase stability of NZSiP/NNFM composite was investigated and is shown in **Figure 6**. The green pellets of mixed cathode with 50:50 wt. ratio of NZSiP and NNFM were sintered at 1,200°C, shrank by 20% laterally and resulted in highly dense composite with approx. 98% of relative density. This is assuming a perfect 50:50 mixture by weight and theoretical densities of 3.27 and 4.11 g/cm³ for NZSiP and NNFM, respectively. The XRD of the polished cross-section of this pellet in **Figure 6** shows the NZSiP and the NNFM phases are fully crystallized after co-sintering at 1,200°C for 10 h in air. However, secondary phases also seem to be forming. The unidentified reflections can be matched with spinel phase $(Ni, Fe, Mn)_3O_4$ (space group 227: Fd-3m; ICSD: 085807) and with Na_2ZrSiO_5 [space group 14: P21/c; (Wilson and Glasser, 1987)]. While the formation of the spinel phase could explain the appearance of a low sodium NNFM phase (described in *Interdiffusion and Side Phases*), neither EDX nor SIMS can detect another phase formation. Therefore, it is more likely, that NZSiP partially crystallizes in the P21/c space group when co-sintered together with NNFM. Further investigation is necessary to understand what this means for the electrochemical performance. Such secondary phases might have a detrimental effect, if they impede the ionic or electronic conductivity or cannot be re-sodiated. After sintering the composite at 1,260°C for 6 h in air, the specimen was deformed, which could be due to a partial melting of either NNFM, NZSiP or a combination of glass-forming elements that do not generate x-ray reflections. This phenomenon is in agreement with the findings of computational studies by Miara et al. for lithium battery materials, where they used lithium potential to predicted the cathode-electrolyte stability (Richards et al., 2016). They observed that generally the electrolyte materials that are predicted to be stable at the cathode voltage show low reaction energies as they come entirely from the mixing of cathode and electrolyte compositions and do not involve redox activity. The same can be translated to increased reactivity and mobility of charge carriers in the NNFM/NZSiP composite at the interface at

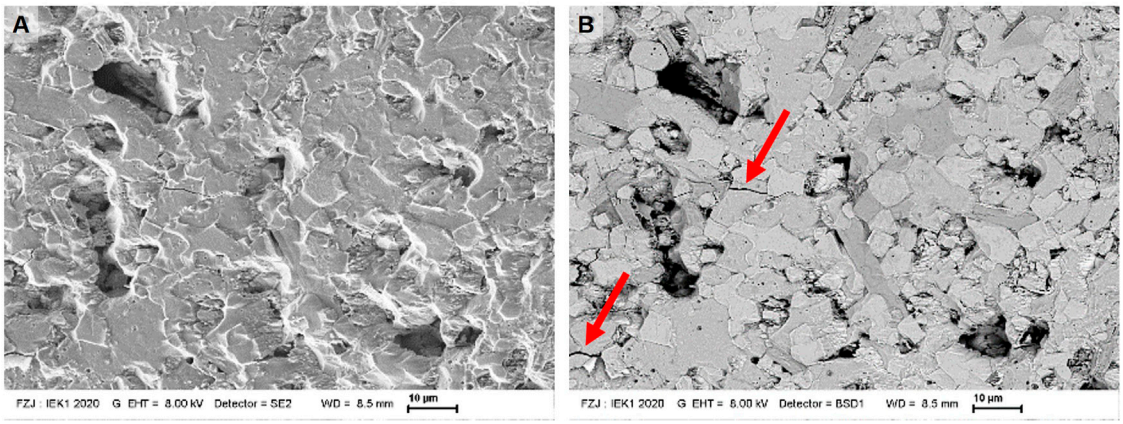

FIGURE 5 | Secondary electron **(A)** and backscattered electron image **(B)** of composite cathode material NNFM/NZSiP. Cracks highlighted by red arrows.

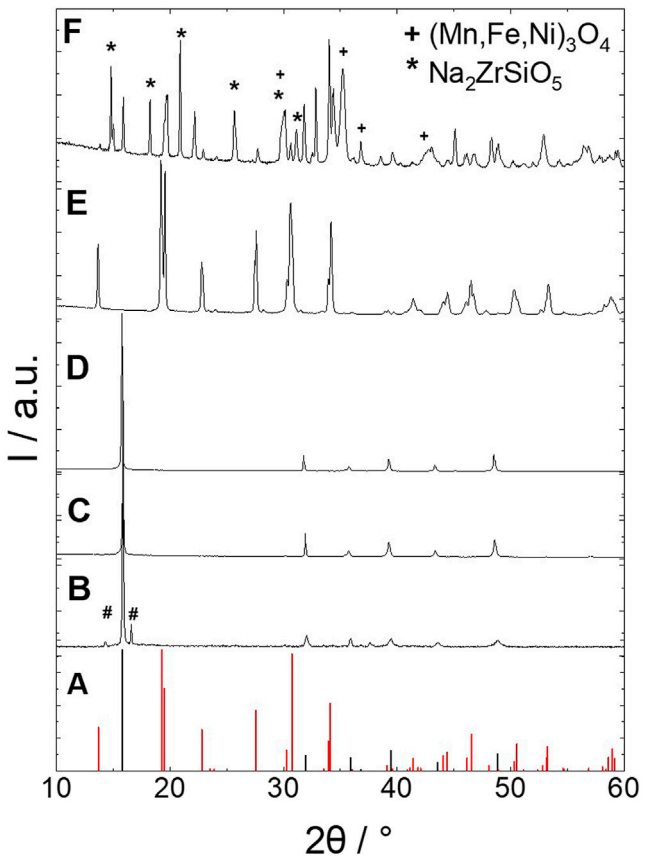

FIGURE 6 | XRD patterns of NNFM heat treated at **(B)** 800°C, **(C)** 1,200°C, **(D)** 1,260°C, **(E)** NZSiP heat treated at 1,260°C and **(F)** NNFM/NZSiP co-sintered at 1,200°C. Stars and pluses highlight secondary phases. For comparison the **(A)** XRD patterns of NNFM (black) and NZSiP (red) are also shown from literature (Ma et al., 2019; Choi et al., 2020).

extreme sintering temperatures. Therefore, we proceeded with our investigation on co-sintered material processed at slightly reduced temperature of 1,200°C.

Microstructure

The microstructure of NNFM/NZSiP composites after sintering at 1,200°C for 10 h in the air is investigated via SEM and shown in **Figure 5**, where a high densification is evident. The two phases NNFM and NZSiP in the composite are clearly distinguishable with a brightness difference in the backscattered scanning electron images (**Figure 5B**). The NZSiP appears slightly brighter compared to the NNFM since it has a higher mean atomic number ($\overline{Z}$(NZSiP) = 20.3 *and* $\overline{Z}$(NNFM) = 17.8). The presence of only a few cracks–which seemingly propagate more through grains rather than along grain boundaries as highlighted by the arrows–and few voids are also visible indicating a relatively good contact between the grains of two phases. The overall microstructure gives an impression that NNFM and NZSiP phases have a good adhesion. The cracks are formed during the cooling step of the sintering process that generates high stresses at the intergranular interface due to the high anisotropic nature of these compounds. The formation of cracks is minimized by a slow cooling rate of 5 K/min and it can also be further reduced.

Interdiffusion and Side Phases

To investigate intergranular diffusion of cations between NNFM and NZSiP or a reaction at their interface, elemental mapping was performed on the polished cross section of NNFM/NZSiP sintered composite using the EDX and TOF SIMS and the results are shown in **Figures 7**, **8**. The major cations of NZSiP are Zr and Si and that of NNFM are Mn, Ni and Fe. In the elemental mapping, a distinct difference between Zr-Si (b-c) and Mn-Ni-Fe (d-f) shows no evidence of intergranular elemental diffusion. Both grains have sharp phase boundaries indicating the likelihood of any reaction is low even though XRD indicates unidentified phases. Both EDX and SIMS show that NASICON phase is uniform throughout the analyzed area. However, the areas where NNFM is expected, Na elemental maps show two distinct regions of higher and lower transition metals concentration, as evident in **Figures 7A,D–F**. These two regions also correlate to varying Na signal as indicated by arrows in EDX mapping **Figure 7A** and SIMS mapping

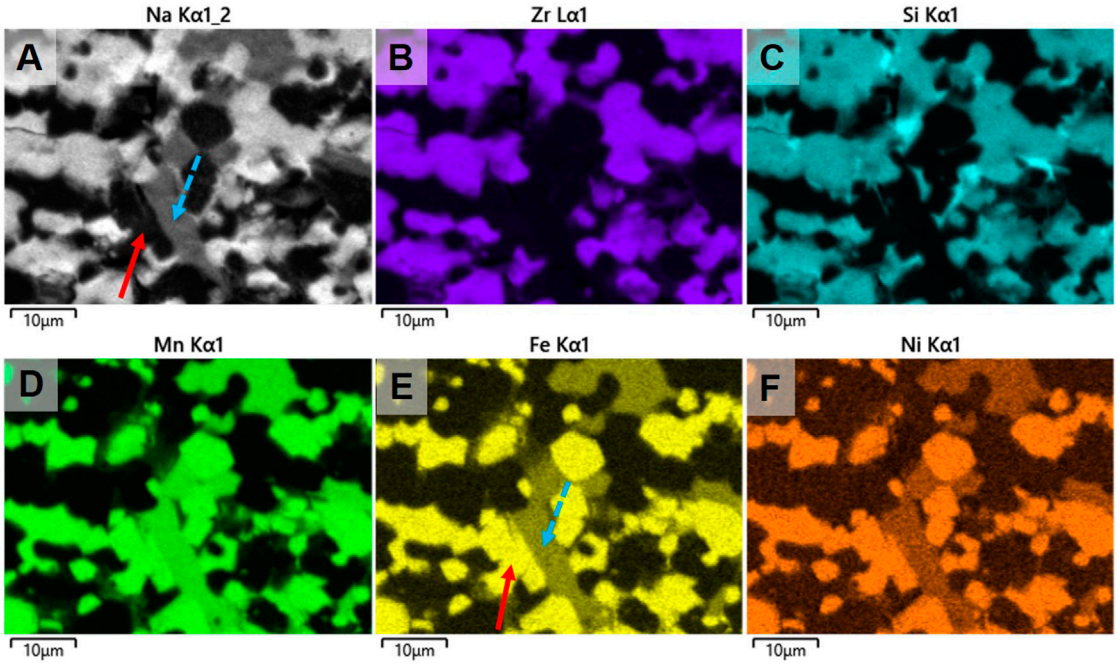

FIGURE 7 | Elemental analysis of NNFM/NaSICON co-sintered specimen using EDX. Arrows highlighting Na rich (blue) and Na poor (red) NNFM regions.

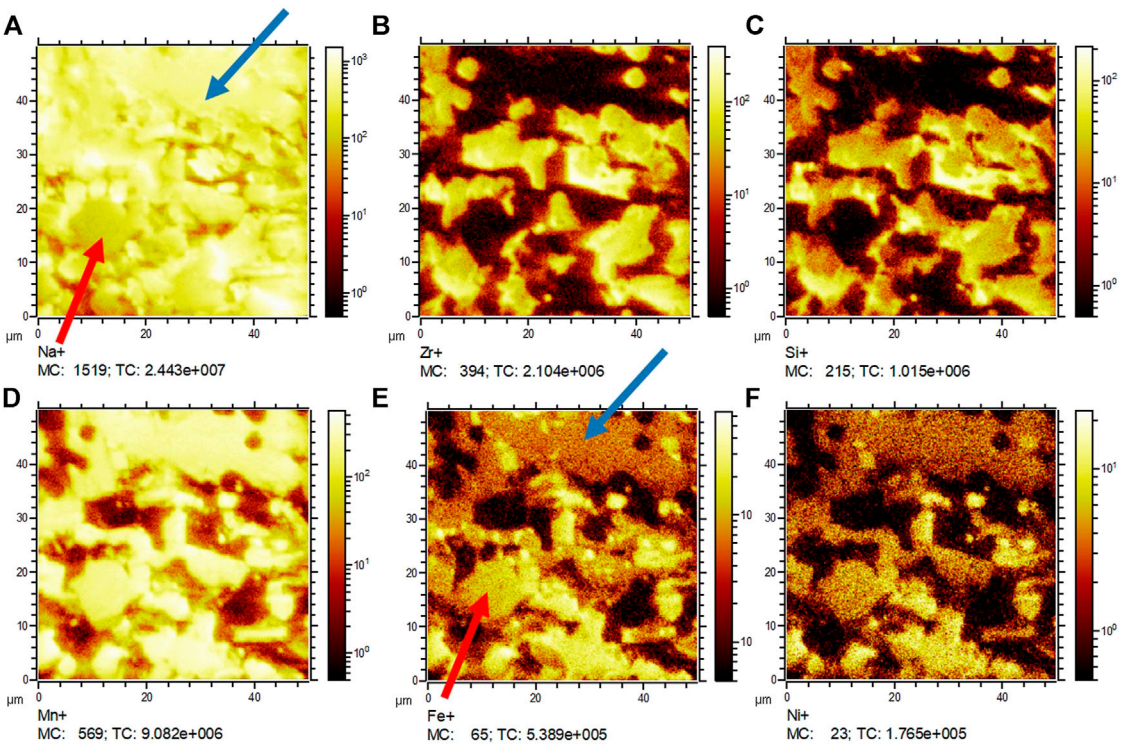

FIGURE 8 | SIMS analysis results of co-sintered NNFM/NZSiP specimen. Arrows highlighting Na rich (blue) and Na poor (red) NNFM regions.

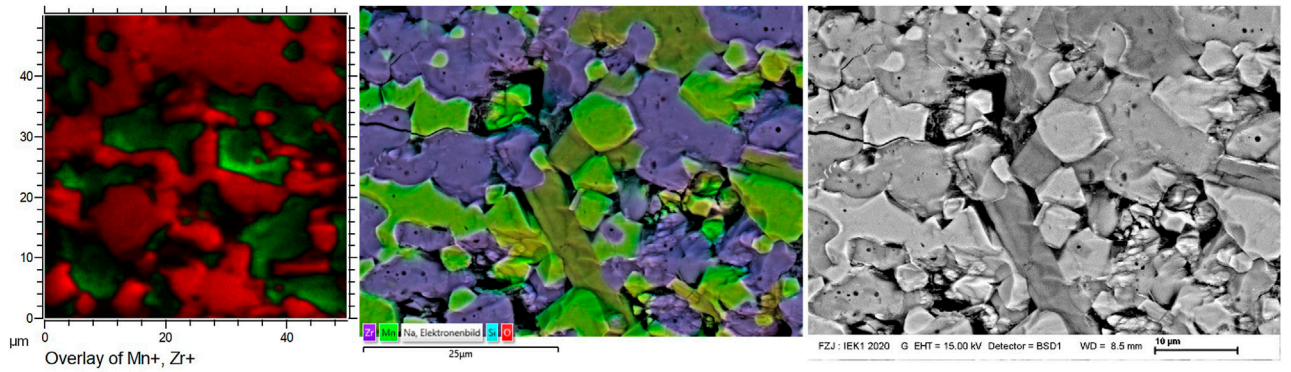

FIGURE 9 | NNFM/NZSiP co-sintered pellet. Overlay of detected elements from SIMS **(left)** and EDX **(middle)**, as well as BSE image **(right)**.

Figure 8A. In EDX images, two distinct phases of NNFM are seen i.e., a Na-containing and non-Na-containing phase. However, in SIMS, which is a more sensitive analysis technique, it is seen as both NNFM phases have Na but of different content. Although stable when sintered individually, apparently the pre-calcined powder crystallizes into a sodium rich NNFM phase and a sodium deficient NNFM when sintered with NaSICON. This is in agreement with XRD findings (**Figure 6**) where an additional phase formation was observed. The lack of sodium could also be partially attributed to its evaporation upon prolonged exposure to high temperatures, which is 10 h at 1,200°C in these samples. Further investigations are however required to fully understand and prevent this phenomenon. Since no diffusion of any other element is observed aside from sodium content, both EDX and SIMS confirm the stability of NZSiP and NNFM. Any reaction of NZSiP and NNFM would have led to intergranular elemental diffusion of elements. This is clearly seen by sharp intergranular boundaries and no concentration gradient when Zr and Mn maps of EDX and SIMS are overlaid in **Figure 9**.

CONCLUSION

We successfully synthesized a pure NNFM as cathode material for all solid state sodium-ion batteries via a relatively cheap and easy processing route SA-SSR. Contrary to conventional sol-gel synthesis, which uses chelating agents such as citric acid and sucrose, we were able to produce phase pure P'2-type $Na_{0.62}[Ni_{0.10}Fe_{0.10}Mn_{0.80}]O_2$ without the need of burning off carbonaceous material and emitting extra CO_2, making this a cheap and industrially scalable method for active materials production for Na-SSBs. The thermal investigations of NNFM found no degradation up to 1,260°C. However, co-sintering NNFM with solid electrolyte NZSiP at 1,260°C led to partial melting, showing similar trends as their Li-counterparts where the active-material/solid-electrolyte mixtures are less stable than the individual components. When sintered at a slightly reduced sintering temperature of 1,200°C for 10 h, the composite cathode shrank by almost 35% in volume. No significant intergranular cracks were observed, which shows that the measured CTE of NNFM, which is 2.5 times that of NZSiP, is within an acceptable range. The elemental mapping performed via EDX and SIMS confirm that NZSiP and NNFM do not react during sintering, however, NNFM forms a sodium rich and a sodium deficient phase. Further investigation is required to understand this phenomenon and its impact on the electrochemical behaviour of the cathode, which will be investigated in the future. In conclusion, NNFM appears to be a promising candidate for fabricating mixed cathodes for all-solid-state sodium-ion battery as it can be co-sintered together with most promising NASICON type NZSiP.

DATA AVAILABILITY STATEMENT

The original contributions presented in the study are included in the article/Supplementary Material, further inquiries can be directed to the corresponding author.

AUTHOR CONTRIBUTIONS

GD and SN designed the experiments, synthesized the materials and are main authors of the manuscript. SN and UB gave excess to and performed SIMS measurements and analysis. MF, OG and DF edited the manuscript and gave valuable advice. All authors approved the submitted version.

FUNDING

Helmholtz Association and the Federal Ministry of Education and Research (BMBF) within the MEET-HiEnD III project (Grant No. 13XP0258B) and the project MiTemp (Grant No. 13XP0183B).

ACKNOWLEDGMENTS

The authors would like to thank D. Sebold, Y. J. Sohn, DI M-T Gerhards at IEK-1 for SEM, XRD and thermal investigations, respectively. We also thank Volker Nischwitz at ZEA-3 for ICP-OES analysis.

REFERENCES

Avicenne (2020). "*The Rechargeable Battery Market 2019-2030*". 28th (2020) ed. Paris: Avicenne Energy).

Choi, J. U., Jo, J. H., Park, Y. J., Lee, K. S., and Myung, S. T. (2020). Mn-Rich P′2-$Na_{0.67}[Ni_{0.1}Fe_{0.1}Mn_{0.8}]O_2$ as High-Energy-Density and Long-Life Cathode Material for Sodium-Ion Batteries. *Adv. Energ. Mater.* 10 (27), 1–10. doi:10.1002/aenm.202001346

Choi, J. U., Park, Y. J., Jo, J. H., Kuo, L.-Y., Kaghazchi, P., and Myung, S.-T. (2018). Unraveling the Role of Earth-Abundant Fe in the Suppression of Jahn-Teller Distortion of P′2-Type Na2/3MnO2: Experimental and Theoretical Studies. *ACS Appl. Mater. Inter.* 10, 40978–40984. doi:10.1021/acsami.8b16522

Choi, J. U., Yoon, C. S., Zhang, Q., Kaghazchi, P., Jung, Y. H., Lee, K.-S., et al. (2019). Understanding on the Structural and Electrochemical Performance of Orthorhombic Sodium Manganese Oxides. *J. Mater. Chem. A.* 7, 202–211. doi:10.1039/c8ta08796b

Dellen, C., Gehrke, H.-G., Möller, S., Tsai, C.-L., Breuer, U., Uhlenbruck, S., et al. (2016). Time-of-flight Secondary Ion Mass Spectrometry Study of Lithium Intercalation Process in LiCoO2 Thin Film. *J. Power Sourc.* 321, 241–247. doi:10.1016/j.jpowsour.2016.04.084

Doeff, M. M., Visco, S. J., Yanping, M., Peng, M., Lei, D., and De Jonghe, L. C. (1995). Thin Film Solid State Sodium Batteries for Electric Vehicles. *Electrochimica Acta* 40, 2205–2210. doi:10.1016/0013-4686(95)00164-a

Finsterbusch, M., Danner, T., Tsai, C.-L., Uhlenbruck, S., Latz, A., and Guillon, O. (2018). High Capacity Garnet-Based All-Solid-State Lithium Batteries: Fabrication and 3D-Microstructure Resolved Modeling. *ACS Appl. Mater. Inter.* 10, 22329–22339. doi:10.1021/acsami.8b06705

Gao, H., Xin, S., Xue, L., and Goodenough, J. B. (2018). Stabilizing a High-Energy-Density Rechargeable Sodium Battery with a Solid Electrolyte. *Chem.* 4, 833–844. doi:10.1016/j.chempr.2018.01.007

Gopalakrishnan, J., and Rangan, K. K. (1992). Vanadium Phosphate (V2(PO4)3): a Novel NASICO N-type Vanadium Phosphate Synthesized by Oxidative Deintercalation of Sodium from Sodium Vanadium Phosphate (Na3V2(PO4)3). *Chem. Mater.* 4, 745–747. doi:10.1021/cm00022a001

Gordon, S., and Campbell, C. (1955). Differential Thermal Analysis of Inorganic Compounds. *Anal. Chem.* 27, 1102–1109. doi:10.1021/ac60103a018

Iltgen, K., Bendel, C., Benninghoven, A., and Niehuis, E. (1997). Optimized Time-Of-Flight Secondary Ion Mass Spectroscopy Depth Profiling with a Dual Beam Technique. *J. Vacuum Sci. Tech. A: Vacuum, Surf. Films* 15, 460–464. doi:10.1116/1.580874

Inoishi, A., Omuta, T., Kobayashi, E., Kitajou, A., and Okada, S. (2017). A Single-phase, All-Solid-State Sodium Battery Using $Na_{3-x}V_{2-x}Zr_x(PO_4)_3$ as the Cathode, Anode, and Electrolyte. *Adv. Mater. Inter.* 4 (5), 1–5. doi:10.1002/admi.201600942

Kumakura, S., Tahara, Y., Kubota, K., Chihara, K., and Komaba, S. (2016). Sodium and Manganese Stoichiometry of P2-type Na2/3 MnO2. *Angew. Chem. Int. Ed.* 55, 12760–12763. doi:10.1002/anie.201606415

Lalère, F., Leriche, J. B., Courty, M., Boulineau, S., Viallet, V., Masquelier, C., et al. (2014). An All-Solid State NASICON Sodium Battery Operating at 200 °C. *J. Power Sourc.* 247, 975–980. doi:10.1016/j.jpowsour.2013.09.051

Lan, T., Tsai, C.-L., Tietz, F., Wei, X.-K., Heggen, M., Dunin-Borkowski, R. E., et al. (2019). Room-temperature All-Solid-State Sodium Batteries with Robust Ceramic Interface between Rigid Electrolyte and Electrode Materials. *Nano Energy* 65, 1–9. doi:10.1016/j.nanoen.2019.104040

Larcher, D., and Tarascon, J.-M. (2015). Towards Greener and More Sustainable Batteries for Electrical Energy Storage. *Nat. Chem.* 7, 19–29. doi:10.1038/nchem.2085

Liu, L., Qi, X., Ma, Q., Rong, X., Hu, Y.-S., Zhou, Z., et al. (2016). Toothpaste-like Electrode: A Novel Approach to Optimize the Interface for Solid-State Sodium-Ion Batteries with Ultralong Cycle Life. *ACS Appl. Mater. Inter.* 8, 32631–32636. doi:10.1021/acsami.6b11773

Ma, Q., Guin, M., Naqash, S., Tsai, C.-L., Tietz, F., and Guillon, O. (2016). Scandium-Substituted Na3Zr2(SiO4)2(PO4) Prepared by a Solution-Assisted Solid-State Reaction Method as Sodium-Ion Conductors. *Chem. Mater.* 28, 4821–4828. doi:10.1021/acs.chemmater.6b02059

Ma, Q., and Tietz, F. (2020). Solid-State Electrolyte Materials for Sodium Batteries: Towards Practical Applications. *ChemElectroChem* 7, 2693–2713. doi:10.1002/celc.202000164

Ma, Q., Tsai, C.-L., Wei, X.-K., Heggen, M., Tietz, F., and Irvine, J. T. S. (2019). Room Temperature Demonstration of a Sodium Superionic Conductor with Grain Conductivity in Excess of 0.01 S Cm−1 and its Primary Applications in Symmetric Battery Cells. *J. Mater. Chem. A.* 7, 7766–7776. doi:10.1039/c9ta00048h

Mckissock, B., Loyselle, P., and Vogel, E. (2008). *Guidlines on Lithium-Ion Battery Use in Space Applications*. Cleveland, Ohio): Glenn Research Center.

Minakshi, M., and Ralph, D. (2013). A Novel Sodium-Ion Rechargeable Battery. *ECS Trans.* 45, 95–102. doi:10.1149/04529.0095ecst

Mücke, R., Finsterbusch, M., Kaghazchi, P., Fattakhova-Rohlfing, D., and Guillon, O. (2021). Modelling Electro-Chemical Induced Stresses in All-Solid-State Batteries: Anisotropy Effects in Cathodes and Cell Design Optimisation. *J. Power Sourc.* 489, 1–9. doi:10.1016/j.jpowsour.2020.229430

Naqash, S., Gerhards, M.-T., Tietz, F., and Guillon, O. (2018). Coefficients of Thermal Expansion of Al- and Y-Substituted NaSICON Solid Solution Na3+2xAlxYxZr2−2xSi2PO12. *Batteries* 4. doi:10.3390/batteries4030033

Parant, J.-P., Olazcuaga, R., Devalette, M., Fouassier, C., and Hagenmuller, P. (1971). Sur quelques nouvelles phases de formule NaxMnO2 (x ⩽ 1). *J. Solid State. Chem.* 3, 1–11. doi:10.1016/0022-4596(71)90001-6

Peters, J., Buchholz, D., Passerini, S., and Weil, M. (2016). Life Cycle Assessment of Sodium-Ion Batteries. *Energy Environ. Sci.* 9, 1744–1751. doi:10.1039/c6ee00640j

Peters, J. F., Peña Cruz, A., and Weil, M. (2019). Exploring the Economic Potential of Sodium-Ion Batteries. *Batteries* 5 (1), 1–15. doi:10.3390/batteries5010010

Richards, W. D., Miara, L. J., Wang, Y., Kim, J. C., and Ceder, G. (2016). Interface Stability in Solid-State Batteries. *Chem. Mater.* 28, 266–273. doi:10.1021/acs.chemmater.5b04082

Stoyanova, R., Carlier, D., Sendova-Vassileva, M., Yoncheva, M., Zhecheva, E., Nihtianova, D., et al. (2010). Stabilization of Over-stoichiometric Mn4+ in Layered Na2/3MnO2. *J. Solid State. Chem.* 183, 1372–1379. doi:10.1016/j.jssc.2010.04.024

Wilson, G., and Glasser, F. P. (1987). *Powder Diffraction, Vol. 2 (3)*. Cambridge: Cambridge University Press, 176–179. doi:10.1117/12.941148

Yabuuchi, N., Kubota, K., Dahbi, M., and Komaba, S. (2014). Research Development on Sodium-Ion Batteries. *Chem. Rev.* 114, 11636–11682. doi:10.1021/cr500192f

Yuvaraj, S., Fan-Yuan, L., Tsong-Huei, C., and Chuin-Tih, Y. (2003). Thermal Decomposition of Metal Nitrates in Air and Hydrogen Environments. *J. Phys. Chem. B.* 107, 1044–1047. doi:10.1021/jp026961c

Zeng, X., Li, M., Abd El-Hady, D., Alshitari, W., Al-Bogami, A. S., Lu, J., et al. (2019). Commercialization of Lithium Battery Technologies for Electric Vehicles. *Adv. Energ. Mater.* 9 (27), 1–25. doi:10.1002/aenm.201900161

Zhang, Z., Zhang, Q., Shi, J., Chu, Y. S., Yu, X., Xu, K., et al. (2017). A Self-Forming Composite Electrolyte for Solid-State Sodium Battery with Ultralong Cycle Life. *Adv. Energ. Mater.* 7 (4), 1–11. doi:10.1002/aenm.201601196

Zubi, G., Dufo-López, R., Carvalho, M., and Pasaoglu, G. (2018). The Lithium-Ion Battery: State of the Art and Future Perspectives. *Renew. Sustain. Energ. Rev.* 89, 292–308. doi:10.1016/j.rser.2018.03.002

Conflict of Interest: The authors declare that the research was conducted in the absence of any commercial or financial relationships that could be construed as a potential conflict of interest.